5-15-2021

Structural alterations in cortical and thalamocortical white matter tracts after recovery from prefrontal cortex lesions in macaques

Ramina Adam
The University of Western Ontario

David J. Schaeffer
University of Pittsburgh

Kevin Johnston
The University of Western Ontario

Ravi S. Menon
Robarts Research Institute

Stefan Everling
The University of Western Ontario

Citation of this paper:
Ramina Adam, David J. Schaeffer, Kevin Johnston, Ravi S. Menon, Stefan Everling, Structural alterations in cortical and thalamocortical white matter tracts after recovery from prefrontal cortex lesions in macaques, NeuroImage, Volume 232, 2021, 117919, ISSN 1053-8119, https://doi.org/10.1016/j.neuroimage.2021.117919. (https://www.sciencedirect.com/science/article/pii/S1053811921001968)

NeuroImage 232 (2021) 117919

Contents lists available at ScienceDirect

NeuroImage

journal homepage: www.elsevier.com/locate/neuroimage

Structural alterations in cortical and thalamocortical white matter tracts after recovery from prefrontal cortex lesions in macaques

Ramina Adam[a,b,c], David J. Schaeffer[d], Kevin Johnston[c,e], Ravi S. Menon[b,c,f], Stefan Everling[a,b,c,e,*]

[a] Graduate Program in Neuroscience, University of Western Ontario, London, Canada
[b] Robarts Research Institute, University of Western Ontario, London, Canada
[c] The Brain and Mind Institute, University of Western Ontario, London, Canada
[d] Department of Neurobiology, University of Pittsburgh, PA, United States
[e] Department of Physiology and Pharmacology, University of Western Ontario, London, Canada
[f] Department of Medical Biophysics, University of Western Ontario, London, Canada

ARTICLE INFO

Keywords:
Diffusion MRI
Probabilistic tractography
Saccades
Target selection
Endothelin-1
Nonhuman primates

ABSTRACT

Unilateral damage to the frontoparietal network typically impairs saccade target selection within the contralesional visual hemifield. Severity of deficits and the degree of recovery have been associated with widespread network dysfunction, yet it is not clear how these behavioural and functional brain changes relate with the underlying structural white matter tracts. Here, we investigated whether recovery after unilateral prefrontal cortex (PFC) lesions was associated with changes in white matter microstructure across large-scale frontoparietal cortical and thalamocortical networks. Diffusion-weighted imaging was acquired in four male rhesus macaques at pre-lesion, week 1, and week 8-16 post-lesion when target selection deficits largely recovered. Probabilistic tractography was used to reconstruct cortical frontoparietal fiber tracts, including the superior longitudinal fasciculus (SLF) and transcallosal fibers connecting the PFC or posterior parietal cortex (PPC), as well as thalamocortical fiber tracts connecting the PFC and PPC to thalamic nuclei. We found that the two animals with small PFC lesions showed increased fractional anisotropy in both cortical and thalamocortical fiber tracts when behaviour had recovered. However, we found that fractional anisotropy decreased in cortical frontoparietal tracts after larger PFC lesions yet increased in some thalamocortical tracts at the time of behavioural recovery. These findings indicate that behavioural recovery after small PFC lesions may be supported by both cortical and subcortical areas, whereas larger PFC lesions may have induced widespread structural damage and hindered compensatory remodeling in the cortical frontoparietal network.

1. Introduction

Impaired spatial attention and reduced gaze shifts toward the contralesional visual hemifield are commonly seen following unilateral damage to a primate frontoparietal network, which includes the caudal prefrontal cortex (PFC), posterior parietal cortex (PPC), and white matter pathways connecting these areas within a large-scale network (Mesulam, 1999; Corbetta and Shulman, 2011; Bartolomeo et al., 2012). In stroke patients, these deficits manifest as a decreased ability to respond or attend to a single visual target within the contralesional hemifield, a phenomenon known as visual neglect (Bartolomeo, 2007; Li and Malhotra, 2015). In many cases, deficits within the contralesional hemifield appear only in the presence of a competing ipsilesional stimulus, referred to as visual extinction (Di Pellegrino et al., 1997; de Haan et al., 2012a). Similar impairments have been demonstrated in macaque monkeys after lesions or reversible inactivation of PFC or PPC areas (Latto and Cowey, 1971; Lynch and Mclaren, 1989; Schiller and Chou, 1998; Wardak et al., 2002, 2004, 2006; Wilke et al., 2012; Johnston et al., 2016; Adam et al., 2019). Functional imaging studies in stroke patients and animal lesion models have shown that functional changes across a distributed network correlated with the severity of lateralized deficits in the acute stage (Umarova et al., 2011; Wilke et al., 2012; Baldassarre et al., 2014) and with the degree of recovery in the chronic stage (Deuel and Collins, 1983; He et al., 2007; Ramsey et al., 2016; Umarova et al., 2016).

Recently, we reported the longitudinal changes in resting-state functional connectivity (rsFC) within a frontoparietal network after unilateral caudal lateral PFC lesions in macaque monkeys (Adam et al., 2020).

* Corresponding author at: Centre for Functional and Metabolic Mapping, Robarts Research Institute, 1151 Richmond Street North, London, ON N6A 5B7, Canada.
E-mail address: severlin@uwo.ca (S. Everling).

https://doi.org/10.1016/j.neuroimage.2021.117919
Received 8 June 2020; Received in revised form 19 February 2021; Accepted 22 February 2021
Available online 27 February 2021

We found that recovery of contralesional target selection correlated with increasing rsFC between contralesional PFC and ipsilesional PPC. Since network-wide rsFC has been shown to reflect properties of underlying structural connections (Hagmann et al., 2008; Greicius et al., 2009; Dijkhuizen et al., 2012; Shen et al., 2015), here we expand on our previous study to examine the structural changes in white matter pathways connecting the frontoparietal network, including bilateral superior longitudinal fasciculus (SLF) and transcallosal fibers connecting bilateral PFC and bilateral PPC. The SLF is a long-range association pathway connecting frontoparietal areas within hemisphere (Petrides and Pandya, 1984; Schmahmann et al., 2007; Thiebaut de Schotten et al., 2012). Between hemispheres, the PFC and PPC are connected to their respective contralateral homologs via transcallosal fibers crossing at the genu or isthmus of the corpus callosum, respectively (Barbas and Pandya, 1984; Hofer et al., 2008). However, it is possible that behavioural compensation after larger lesions may not be solely mediated by cortical connections, but may instead depend on a functionally-related third region or network (Damoiseaux and Greicius, 2009). Thus, we further explored the effects of PFC lesions on thalamocortical fiber tracts connecting frontoparietal cortical areas to thalamic nuclei. The superior colliculus sends indirect projections to the FEF in the caudal PFC via the mediodorsal nucleus of the thalamus (Barbas and Mesulam, 1981; Goldman-Rakic and Porrino, 1985; Kievit and Kuypers, 1977; Sommer and Wurtz, 2004) and to area LIP in the PPC via the lateral pulvinar (Asanuma et al., 1985; Baizer et al., 1993; Selemon and Goldman-Rakic, 1988). Moreover, these thalamic nuclei have been shown to play a role in visuospatial attention (Petersen et al., 1987; Sommer and Wurtz, 2004), which supports a potential role in the recovery of saccade target selection.

It has not yet been explored whether recovery of contralesional target selection after focal lesions is associated with changes in white matter fibers. Moreover, the behavioural relevance of structural alterations in remote fiber tracts before and after focal damage are not well understood. Here, we examined microstructural changes of white matter tracts in four macaque monkeys using high resolution diffusion-weighted imaging (DWI) acquired *in vivo* at 7T. DWI data were obtained before the PFC lesions were induced, at week 1 post-lesion, and at week 8-16 post-lesion, when contralesional target selection had largely recovered. Probabilistic tractography was used to reconstruct contralesional/ipsilesional SLF and transcallosal PFC and PPC tracts which were then used to obtain tract-specific diffusion parameters, including fractional anisotropy (FA). We speculated that remote fiber tracts (i.e., contralesional SLF and transcallosal PPC) may have mediated the increased rsFC between contralesional PFC and ipsilesional PPC found in our previous study (Adam et al., 2020), since those tracts provide an undamaged pathway indirectly linking the cortical regions together. We hypothesized that the distant contralesional SLF and transcallosal PPC tracts play a compensatory role to support behavioural recovery by mediating the increased rsFC within the affected frontoparietal network. We predicted that if behaviour or rsFC relied on contralesional SLF and transcallosal PPC tracts, then FA within one or both of those remote tracts should increase throughout behavioural recovery.

2. Methods

2.1. Subjects

Data were collected from four adult male macaque monkeys (*Macaca mulatta*) aged 5 – 7 years old and weighing 7 – 10 kg. All surgical and experimental procedures were carried out in accordance with the Canadian Council of Animal Care policy on the use of laboratory monkeys and approved by the Animal Care Committee of the University of Western Ontario Council. Experimental methods for these subjects has been previously published in our companion paper (Adam et al., 2020). Herein, animals are individually described as Monkey L, Monkey S, Monkey B, and Monkey F. We show behavioural data from these subjects at the following time points: pre-lesion, week 1-2 post-lesion (early post-lesion), and week 8 or 16 post-lesion (late post-lesion). The early post-lesion time point shows the acute behavioural deficits following the lesion and the late post-lesion time point shows the recovered behaviour months later. DWI data was acquired at pre-lesion and post-lesion (described below) to examine how the white matter microstructure changed at the time of behavioural recovery.

2.2. Lesions

Details of the experimental lesioning surgeries have been previously published in these subjects (Adam et al., 2020). Briefly, lesions were induced using the vasoconstrictor endothelin-1, which induces focal occlusion with subsequent reperfusion and has been validated in marmosets and macaque monkeys (Teo and Bourne, 2014; Herbert et al., 2015; Murata and Higo, 2016; Dai et al., 2017). Intracortical injections were made in the right caudal PFC (along the anterior bank of the arcuate sulcus and the caudal portion of the principal sulcus). We varied the total amount of endothelin-1 administered to each animal to produce small lesions in Monkey L and Monkey S (6-12 μg) and large lesions in Monkey B and Monkey F (16-32 μg). Fig. 1 shows the lesion extent in each animal. All monkeys sustained damage to the right caudal PFC with consistent lesions in area 8AD (Fig. 1B). The lesion in Monkey L was localized to area 8AD and 8B; in Monkey S, the lesion extended further into the dorsolateral and ventrolateral PFC. In Monkey B, the lesion extended into dorsal premotor areas and in Monkey F it extended into the dorsolateral and ventrolateral PFC and premotor areas. Lesion volume analysis showed that Monkey B and Monkey F sustained larger lesions than Monkey L and Monkey S with a lesion volume that was more than doubled (Monkey L = 0.43 cm^3, Monkey S = 0.51 cm^3, Monkey B = 1.28 cm^3, Monkey F = 1.41 cm^3).

2.3. Behaviour

We have previously reported the saccade target selection at pre-lesion and late post-lesion (Adam et al., 2019) but here we compare behavioural performance with DWI data. For a detailed report of the behavioural task design, see (Adam et al., 2019). Before the lesion was induced, monkeys were trained on a saccade task that included two randomly interleaved trial types: (1) visually-guided single target trials and (2) free-choice paired stimulus trials in which a single visual stimulus appeared in each hemifield either simultaneously or at varying stimulus onset asynchronies (SOAs) and monkeys were able to freely select either stimulus as a saccade target to receive a liquid reward (Fig. 2). SOA is the variable temporal delay between presentation of the contralesional and ipsilesional stimulus on the free-choice trials. Each trial began with the presentation of a fixation point, followed by either a single visual target in the contralesional (left) or ipsilesional (right) hemifield or two peripheral stimuli, with one in the contralesional and one in the ipsilesional hemifield presented at a variable SOA. Free-choice trials were used to measure the degree of visual extinction, since contralesional extinction deficits only appear in the presence of a competing ipsilesional stimulus. This task is able to show whether a monkey exhibits a spatially lateralised saccade selection deficit by measuring saccade choice for contralesional and ipsilesional visual stimuli.

In brief, we found that the right caudal PFC lesion induced deficits in contralesional target selection, such that there were decreased correct saccades made towards a single contralesional target (Fig. 3A) and decreased saccade choice of the contralesional stimulus on the free-choice trials (Fig. 3B,C). Deficits gradually recovered over 2-4 months post-lesion. We considered post-lesion behaviour as ‘compensated’ when task performance stabilized without further improvement. The time point for compensated behaviour was week 8 post-lesion for the small lesion monkeys (Monkeys L and S) and week 16 post-lesion for the large lesion monkeys (Monkeys B and F); we refer to these time points collectively

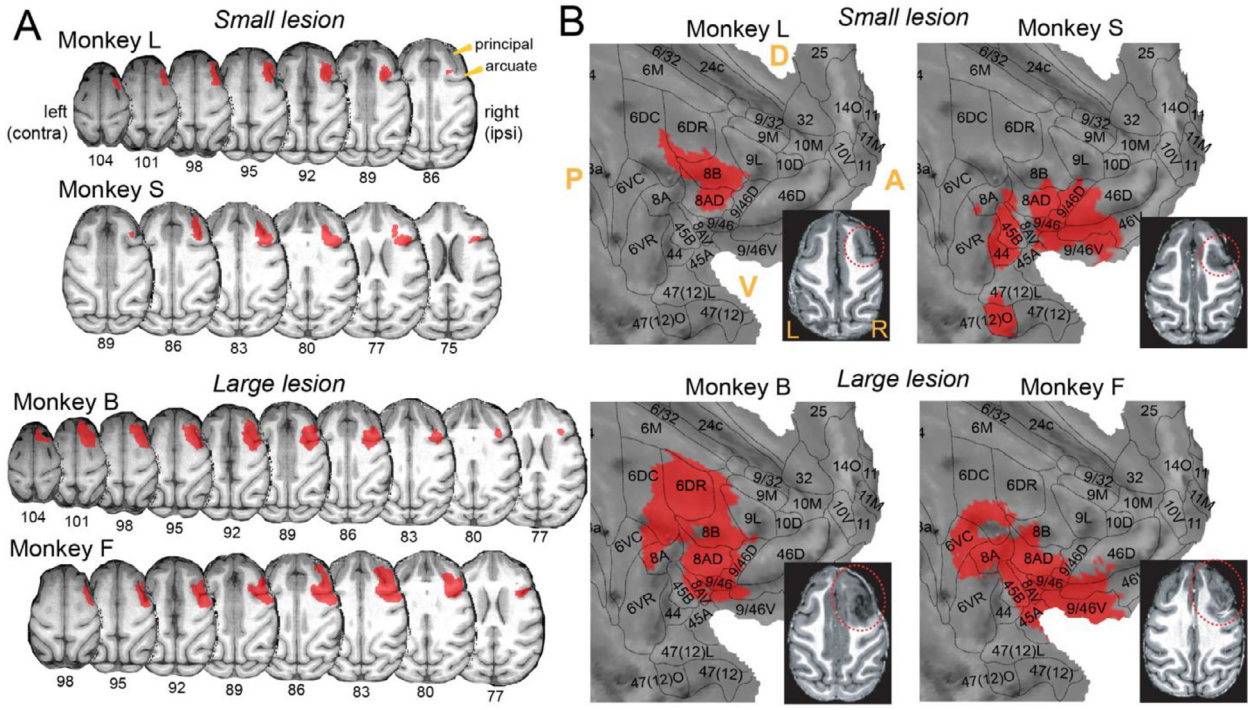

Fig. 1. Lesion masks projected onto the macaque F99 template brain. Each monkey's T1-weighted MP2RAGE anatomical image obtained one week post-lesion was segmented based on tissue type. Masks representing lesioned tissue were registered to the standard macaque F99 space and projected onto (A) axial slices of the macaque F99 brain and (B) cortical flat map representations of the macaque F99 right hemisphere with surface outlines that we created based on the Paxinos et al. (2000) macaque cortical parcellation scheme (Paxinos et al., 2000). Bottom right: one axial T1 image at one week post-lesion showing the lesioned tissue within the dotted red line boundary for each monkey. Abbreviations: principal = principal sulcus; arcuate = arcuate sulcus; contra = contralesional; ipsi = ipsilesional; D = dorsal; V = ventral; A = anterior; P = posterior; L = left; R = right.

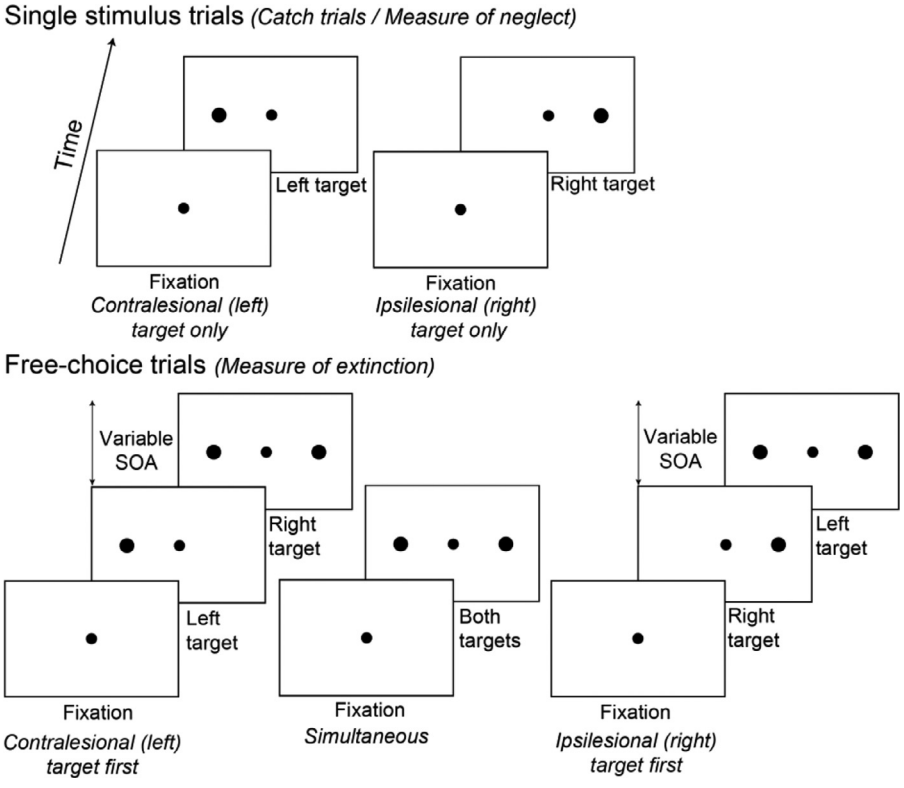

Fig. 2. Behavioural task. Single target and free-choice paired stimulus trials were randomly interleaved within a session. Each trial began with the presentation of a fixation point, followed by either a single target in the contralesional (left) or ipsilesional (right) hemifield or two visual stimuli in either hemifield presented at a variable stimulus onset asynchrony. Stimulus onset asynchrony was the variable temporal delay (0-256 ms) between presentation of the left and right stimulus on the free-choice paired stimulus trials. Abbreviation: SOA = stimulus onset asynchrony.

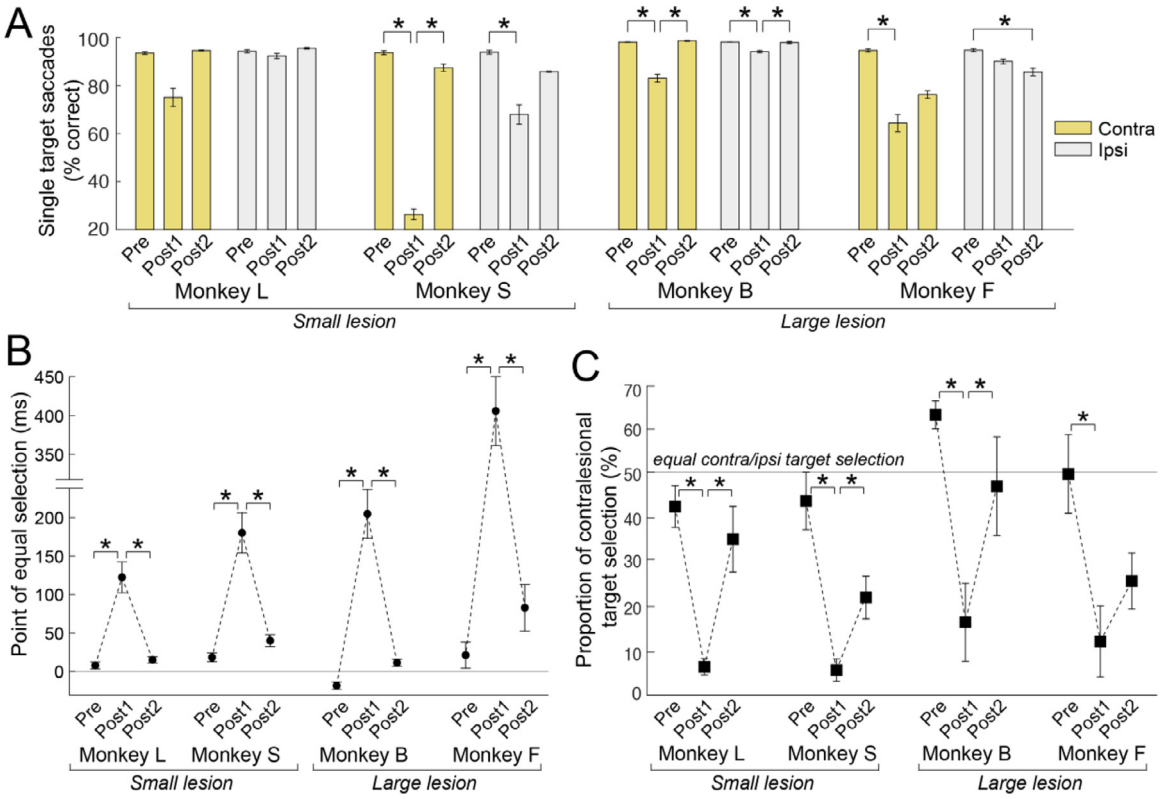

Fig. 3. Saccade target selection deficits and compensation from pre-lesion to early and late post-lesion. (A) The proportion of correct saccades made to a single contralesional (yellow) or ipsilesional (light grey) target. (B) Point of equal selection on the free-choice paired stimulus trials. The point of equal selection is the stimulus onset asynchrony value at which the probability of choosing the contralesional (left) or ipsilesional (right) stimulus was equal. Positive y-axis values indicate that the point of equal selection was reached at a stimulus onset asynchrony in which the contralesional stimulus was presented before the ipsilesional stimulus, which would indicate a contralesional deficit. Negative y-axis values indicate a stimulus onset asynchrony in which the ipsilesional stimulus was presented first. Larger absolute values for the point of equal selection indicates more severe extinction-like deficits. (C) The proportion of saccades made to contralesional stimuli on trials with simultaneous presentation of both stimuli (stimulus onset asynchrony = 0 ms) on the free-choice trials. Statistical comparisons between pre-lesion and post-lesion time points were made using one-way ANOVAs with post-hoc Tukey's tests ($p < 0.05$). Error bars represent standard error of the mean across sessions within each time point. Abbreviations: pre = pre-lesion; post1 = early post-lesion (week 1-2 post-lesion); post2 = late post-lesion (small lesion: week 8 post-lesion; large lesion: week 16 post-lesion); contra = contralesional; ipsi = ipsilesional.

as 'late post-lesion'. Detailed results on this behavioural paradigm have been previously published (Adam et al., 2019, 2020).

2.4. Image acquisition at 7T

One hour prior to scanning, monkeys were sedated with intramuscular injections of 0.05-0.2 mg/kg acepromazine (Acevet 25 mg/ml) and 5.0-7.5 mg/kg ketamine (Vetalar 100 mg/ml), followed by 2.5 mg/kg propofol (10 mg/ml). Monkeys were then intubated with an endotracheal tube and anesthesia was maintained with 1.0-1.5% isoflurane mixed with 100% oxygen. Each monkey was positioned in a custom-built MRI primate bed with its head restrained to reduce motion and then inserted into the magnet bore for image acquisition, at which point the isoflurane level was maintained at 1.0% for the duration of the image acquisition. Body temperature, respiration, heart rate, and blood oxygen saturation levels were continuously monitored and were within a normal range throughout the scans. Body temperature was maintained using thermal insulation and a heating disk.

Imaging data were collected at pre-lesion (after behavioural training), week 1 post-lesion (early post-lesion), and at week 8 or 16 post-lesion when behaviour had compensated near pre-lesion baseline (late post-lesion). Although behaviour had compensated by week 8 for Monkey S, we were only able to obtain DWI data at week 16 post-lesion. Data were acquired on a 7T Siemens MAGNETOM Step 2.3 68-cm horizontal bore scanner (Erlangen, Germany) operating at a slew rate of 300 mT/m/s. We used an in-house designed and manufactured 8-channel transmit, 24-channel receive primate head radiofrequency coil for all image acquisitions (Gilbert et al., 2016). A high-resolution T2-weighted anatomical MR image was acquired using a turbo spin echo sequence with the following parameters: TR = 7500 ms, TE = 80 ms, slices = 42, matrix size = 320 × 320, field of view = 128 × 128 mm, acquisition voxel size = 0.4 mm x 0.4 mm x 1 mm. A T1-weighted MP2RAGE anatomical image was also acquired with these parameters: TR = 6500 ms, TE = 3.15 ms, TI1 = 800 ms, TI2 = 2700 ms, field of view = 128 × 128 mm, 0.5 mm isotropic resolution.

DWI data were obtained using an interleaved echo planar imaging sequence with the following parameters: repetition time (TR) = 5100–7500 ms, echo time (TE) = 46.8–54.8 ms, number of averages = 1, number of slices = 46–54, slice thickness = 1 mm, in-plane resolution = 1 mm x 1 mm. We acquired 64 diffusion-encoding directions (b-value = 1000-1500 s/mm^2) and one non-diffusion weighted volume (b-value = 0 s/mm^2). Although there are slight within-subject variations in our TR (maximal difference of 1500 ms) and TE (maximal difference of 3 ms), previous work has shown no significant differences in the overall magnitude of diffusion between scans with larger differences in TR and TE (Celik, 2016). It has also been demonstrated that the mean FA in high angular resolution scans (e.g., 64 diffusion directions) was not significantly different between scans with a TR of 4000 ms or 13200 ms (Provenzale et al., 2018).

2.5. Image processing

Raw DWI data were converted from DICOM to NIFTI using MRIconvert (Lewis Center for Neuroimaging, University of Oregon) and reoriented to standard space using the FMRIB Software Library (FSL; http://www.fmrib.ox.ac.uk) tools 'fslswapdim' and 'fslorient'. ASCII text files containing a list of gradient directions and b-values for each volume were also flipped and transposed to correspond with the reoriented DWI data. Data processing was then carried out using FMRIB's Diffusion Toolbox (FDT) implemented with FSL. First, eddy current-induced distortions and subject motion were corrected using 'EDDY' (Andersson and Sotiropoulos, 2016). We then performed a diffusion tensor imaging (DTI) analysis to obtain the scalar maps representing FA and mean diffusivity. DTI analysis involved fitting a tensor model at each voxel using 'DTIFIT' on the eddy corrected DWI data. The output DTI scalar maps are directly related to the three major eigenvalues (λ_1, λ_2, λ_3) of the fitted tensor (i.e., the magnitude of diffusion for each eigenvector of the tensor). Mean diffusivity represents the total magnitude of diffusion and is the average of all three eigenvalues. FA represents the degree of anisotropy and is calculated as the relative difference of the first eigenvalue compared to the other two eigenvalues (Basser et al., 1994; Basser and Pierpaoli, 1996; Beaulieu, 2002; Alexander et al., 2007).

Next, a multiple tensor model was fit at each voxel using 'BEDPOSTX' which estimates two fiber orientations per voxel to account for crossing fibers and more accurately generate probability distributions of local fiber orientations (Behrens et al., 2003b, 2007). This Bayesian estimation of multiple fiber directions vastly improves sensitivity when fiber tracking non-dominant pathways through regions of crossing fibers, such as the SLF (anterior-posterior) that has been traditionally difficult to track due to crossing dorsal-ventral projections in the more dominant corona radiata white matter bundle (Behrens et al., 2007). Transformation matrices were derived within subjects for each session from diffusion space to pre-lesion structural T2 space using a rigid-body transformation with 6 degrees of freedom using FSL's 'FLIRT' (Jenkinson et al., 2002). The inverse transformation matrix from this registration was then used to register the seed masks from structural to diffusion space for the probabilistic tractography analysis.

2.6. DWI tractography analysis

2.6.1. Regions of interest for tractography

We reconstructed cortical and thalamocortical fiber tracts using seed regions (radius = 2 mm) created in pre-lesion structural T2 space for each subject. Seed locations were determined using the (Saleem and Logothetis, 2006) rhesus monkey anatomical atlas. Cortical seeds were placed in the frontal eye field (FEF) of the caudal PFC and in the lateral intraparietal area (LIP) of the PPC (Fig. 4). FEF seeds were placed in the anterior bank of the arcuate sulcus (Tehovnik et al., 2000) and LIP seeds were in the lateral bank of the intraparietal sulcus (Lewis and Van Essen, 2000). FEF and LIP constitute the main cortical nodes of the frontoparietal network (Wardak et al., 2011) and have been previously used to track these fibers in rhesus macaques (Hofer et al., 2008). The following seed region pairs were used in a probabilistic tractography analysis (described below) to reconstruct four cortical tracts of interest: bilateral FEF seeds were used to track the transcallosal PFC fiber tracts (Barbas and Pandya, 1984; Hofer et al., 2008); bilateral LIP seeds were used to track the transcallosal PPC tracts (Hofer et al., 2008); contralesional FEF and LIP seeds were used to track the contralesional SLF; and the ipsilesional FEF and LIP seeds were used to track the ipsilesional SLF (Petrides and Pandya, 1984; Schmahmann et al., 2007; Thiebaut de Schotten et al., 2012). A midline sagittal exclusion mask was used to restrict tracking to the opposite hemisphere for the SLF association tracts and an axial exclusion mask at the anterior-posterior midpoint of the corpus callosum was used to restrict tracking to the anterior half of the brain for the transcallosal PFC tract or to the posterior half of the brain for the transcallosal PPC tract.

Thalamic seeds were placed in the mediodorsal nucleus of the thalamus and in the lateral pulvinar (Fig. 4). The superior colliculus sends indirect projections to the FEF via the mediodorsal nucleus of the thalamus (Barbas and Mesulam, 1981; Goldman-Rakic and Porrino, 1985; Kievit and Kuypers, 1977; Sommer and Wurtz, 2004) and to area LIP via the lateral pulvinar (Asanuma et al., 1985; Baizer et al., 1993; Selemon and Goldman-Rakic, 1988). Thus, the following seed region pairs were used to reconstruct thalamocortical fiber tracts: (1) mediodorsal thalamus and FEF and (2) lateral pulvinar and LIP.

2.6.2. Probabilistic tractography

Probabilistic tractography was computed with FDT's 'ProbtrackX' which uses the output from BEDPOSTX to estimate the number of streamlines that traveled between two seed regions for each voxel (Behrens et al., 2003a, 2007). We used the following ProbtrackX standard parameters: number of sample streamlines sent out per seed voxel = 5000, curvature threshold = 0.2, step length = 0.5, maximum number of steps = 2000, subsidiary fibre volume threshold = 0.01. Distance correction was additionally implemented to correct for the decrease in streamlines with distance from the seed region. For each of the 5000 streamlines per seed voxel sampled from the BEDPOSTX probability distribution, a 'successful' streamline was one that originated from one seed and reached the other. This algorithm outputs a streamline density map where individual voxel intensities represent the number of successful streamlines that passed through the voxel. The streamline density map was normalized by dividing it by the waytotal sum, which yielded voxel intensities that now represent the probability of that voxel being part of that tract. In contrast to methods that normalize streamline density maps using a constant proportion of the total number of streamlines sent out per voxel, proportional normalization based on the waytotal sum is the preferred approach when comparing reconstructed fiber tracts across sessions since it accounts for any differences in seeded voxels across sessions that may have affected trackability (Bennett et al., 2011). Streamline probability maps were then thresholded to maintain only voxels with intensities of at least 50% (i.e., a minimum of 50% probability that the voxel belongs to that streamline) and then visually inspected to confirm anatomical plausibility. Note that these suprathreshold white matter voxels are not necessarily exclusively part of the fiber tract of interest, but this probabilistic tractography approach gives a better approximation of the tract-related voxels compared to traditional approaches that use pre-defined region of interest FA mask without tractography. These normalization and thresholding procedures have been used for probabilistic tractography analysis (Galantucci et al., 2011; Latzman et al., 2015; Cunningham et al., 2017; Gray et al., 2018). Thresholded streamline probability maps representing the tracts of interest were generated for each subject and each session individually.

A representative sample of the reconstructed frontoparietal cortical white matter tracts are shown in Fig. 5. These frontoparietal cortical fiber tracts have been previously identified in nonhuman primates using DWI tractography (Schmahmann et al., 2007; Hofer and Frahm, 2008; Hofer et al., 2008; Thiebaut de Schotten et al., 2012; Schaeffer et al., 2017; Sani et al., 2019) and tracer methods (Barbas and Pandya, 1984; Petrides and Pandya, 1984).

Thalamocortical fibers from the mediodorsal nucleus of the thalamus to the PFC travel via the anterior thalamic peduncle and are part of the anterior limb of the internal capsule (Zakszewski et al., 2014). Fibers from lateral pulvinar to the PPC travel via the posterior thalamic peduncle and are part of the posterior limb of the internal capsule. These fiber tracts have been previously identified in humans (Behrens et al., 2003) and nonhuman primates (Zakszewski et al., 2014; Tobias, 1975). A representative sample of the four reconstructed thalamocortical tracts are shown in Fig. 6.

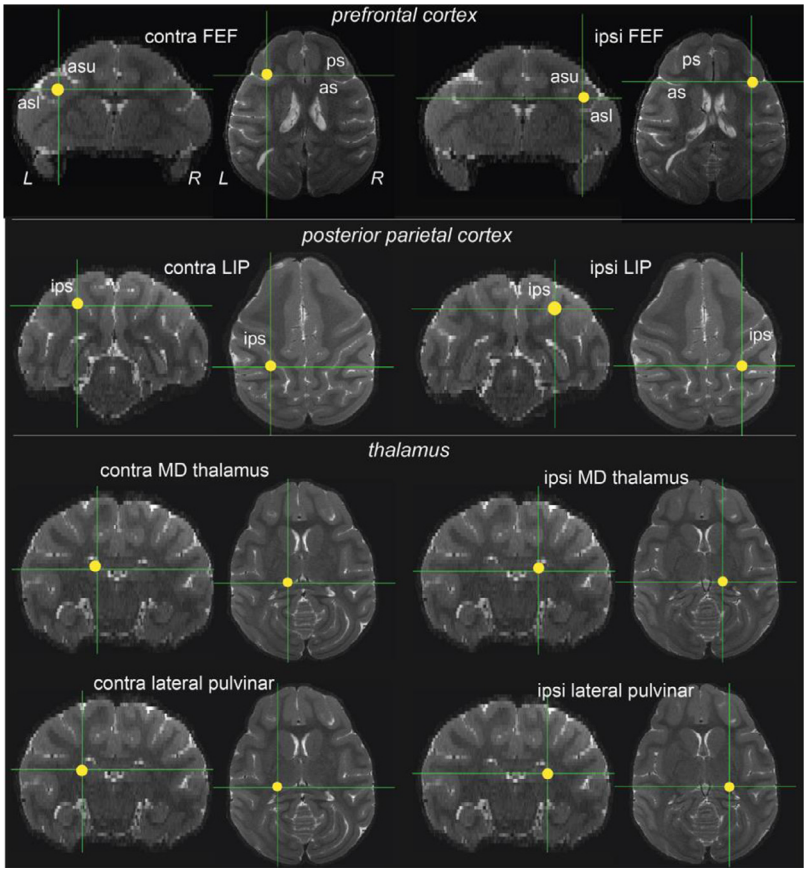

Fig. 4. Seed masks used to reconstruct fiber tracts with probabilistic tractography. Representative bilateral seed regions (shown in yellow) in the FEF, LIP, mediodorsal thalamus, and lateral pulvinar overlaid on coronal and axial T2 sections. Similar seeds were created for each monkey in native pre-lesion T2 space. Abbreviations: L = left, R = right, contra = contralesional, ipsi = ipsilesional, as = arcuate sulcus, asu = upper limb of the arcuate sulcus, asl = lower limb of the arcuate sulcus, ips = intraparietal sulcus, ps = principal sulcus, FEF = frontal eye field, LIP = lateral intraparietal area, PFC = prefrontal cortex, PPC = posterior parietal cortex, MD = mediodorsal.

2.7. Tract-specific DTI parameters

Here, we masked the DTI scalar maps with the reconstructed tracts to obtain tract-specific measures of FA and mean diffusivity at pre-lesion, post-lesion1, and post-lesion2. Previous studies have also obtained tract-specific measures of diffusivity and anisotropy since it takes fiber orientation into account, rather than only measuring diffusion parameters within pre-defined regions of interest without using masks generated from fiber tractography (Bennett et al., 2011; Galantucci et al., 2011; Lindenberg et al., 2012; Ge et al., 2013; Gray et al., 2018). First, the reconstructed thresholded tracts were binarized and only those voxels that overlapped in the binarized tracts from all time points were retained. This conservative approach accounts for any misalignment among individual tracts between time points. For the transcallosal tracts whose diffusion is largely oriented along the left-right x-direction (transcallosal PFC and PPC tracts), voxels within an x-coordinate range that were shared between pre-lesion and late pre-lesion tracts were retained. For the intrahemispheric tracts whose diffusion is largely oriented along the anterior-posterior y-direction, voxels within a shared y-coordinate range in both pre-lesion and late post-lesion tracts were retained. Next, we masked DTI scalar maps with the binarized tracts to obtain tract-wise measures of FA and mean diffusivity. Tract-specific DTI metrics were statistically compared between pre-lesion and post-lesion time points using one-way ANOVAs with post-hoc Tukey's tests ($p < 0.05$) within each subject. Since the SLF has regions of crossing fibers from the corona radiata, we also obtained tract-specific measures from the BEDPOSTX model (*mean_f1samples* and *mean_f2samples*) which estimate the proportion of the diffusion signal that is accounted for by the primary and secondary diffusion directions for the SLF.

3. Results

3.1. Longitudinal changes in the cortical white matter tract DTI parameters

Cortical frontoparietal white matter tracts were reconstructed using probabilistic tractography and used to extract tract-specific diffusion parameters from DTI scalar maps. Average values were calculated across the voxels of each tract and statistically compared between pre-lesion and post-lesion and between early and late post-lesion during behavioural recovery. While we show results from all four cortical tracts at all three time points, our main focus is on the remote fiber tracts that were not directly affected by the lesion, namely the contralesional SLF and transcallosal PPC tracts, and on the changes in FA that occurred throughout behavioural recovery from early to late post-lesion.

In the two small lesion monkeys, Monkeys L and S, one-way ANOVAs revealed that all four cortical frontoparietal tracts showed significantly increased FA from early to late post-lesion throughout behavioural compensation (Fig. 7A,B). Changes in the estimated proportions of the diffusion signal accounted for by the primary and secondary diffusion directions between these time points do not explain the increased FA in the contralesional SLF (see Supplementary Table S1). In other words, the voxels that were isolated as part of the SLF did not become disproportionally more dominated by the primary diffusion direction (i.e., the corona radiata). In Monkey L, mean diffusivity significantly decreased in contralesional SLF from early to late post-lesion (see Supplementary Fig. S1). In Monkey S, mean diffusivity significantly increased in the two lesion-affected transcallosal PFC and ipsilesional SLF tracts from early to late post-lesion (see Supplementary Fig. S1). On the other hand, both

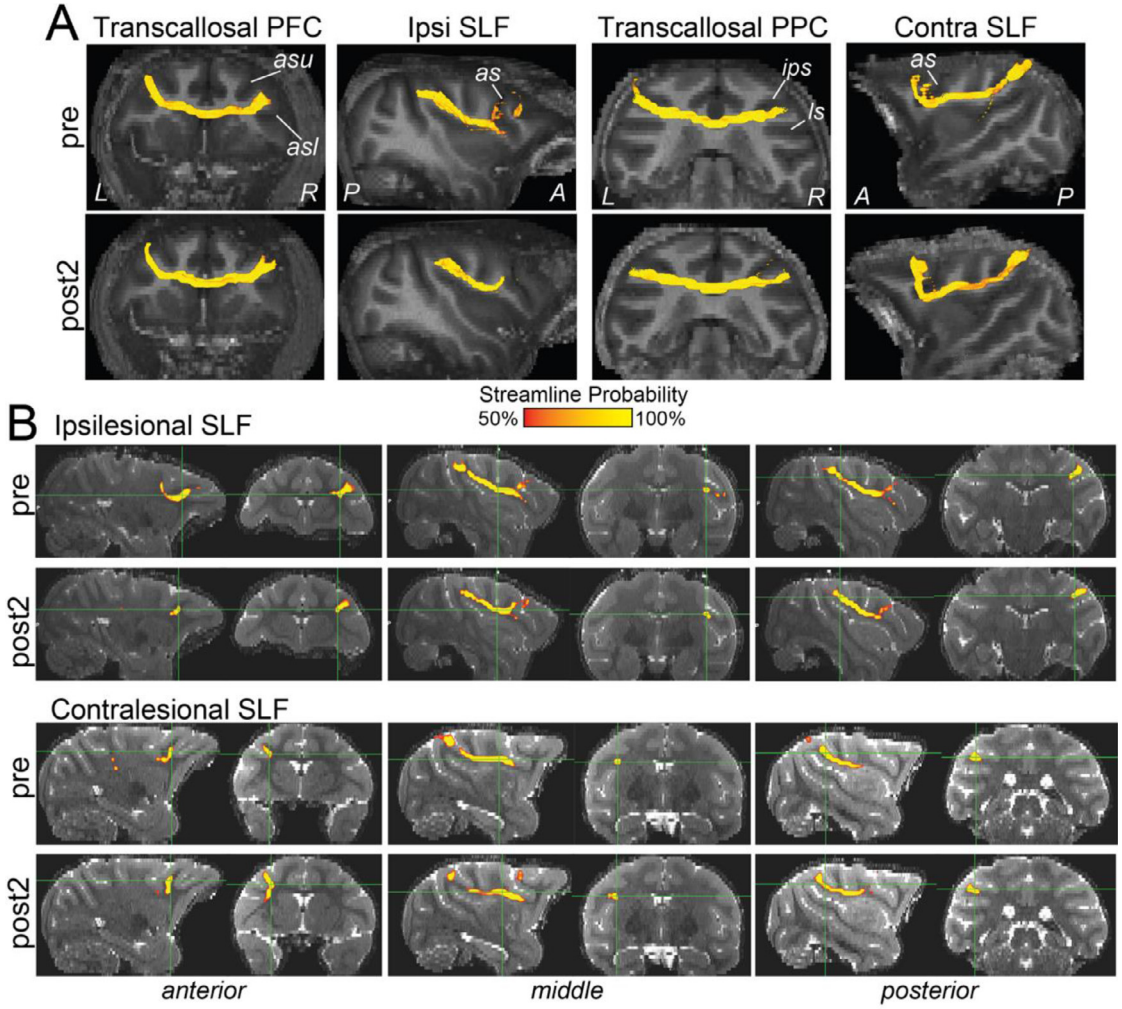

Fig. 5. Representative frontoparietal cortical white matter tracts reconstructed with probabilistic tractography. (A) 3-D tract volumes projected onto a T2 MRI slice. First column: bilateral FEF seeds revealed transcallosal streamlines between the bilateral PFC that traveled across hemispheres through the rostral portion, or genu, of the corpus callosum. Second column: ipsilesional FEF and LIP seeds revealed the ipsilesional SLF association fibers connecting frontal and parietal areas. Third column: bilateral LIP seeds revealed transcallosal streamlines between bilateral PPC that traveled across hemispheres through a posterior region (isthmus) of the corpus callosum. Fourth column: contralesional FEF and LIP seeds revealed the contralesional SLF association fibers connecting frontal and parietal areas. The colour bar represents streamline probabilities for each voxel in the thresholded tracts. (B) Visualization of the bilateral SLF tracts. Anterior, middle, and posterior sections of the SLF tracts are shown overlaid onto sagittal and coronal T2 slices. Abbreviations: pre = pre-lesion, post2 = late post-lesion, A = anterior, P = posterior, L = left, R = right, PFC = prefrontal cortex, PPC = posterior parietal cortex, SLF = superior longitudinal fasciculus, contra = contralesional, ipsi = ipsilesional, as = arcuate sulcus, asu = upper limb of the arcuate sulcus, asl = lower limb of the arcuate sulcus, ips = intraparietal sulcus, ls = lateral sulcus.

monkeys with larger lesions show significantly decreased FA and increased mean diffusivity in cortical frontoparietal tracts (Fig. 7A,B; Supplementary Fig. S1). In Monkey B, decreased FA and increased MD was found in both SLF tracts and in the transcallosal PPC tract, whereas in Monkey F all four tracts showed increased mean diffusivity but only the transcallosal PPC and contralesional SLF showed decreased FA. In sum, FA increased in cortical frontoparietal tracts following small PFC lesions but decreased following larger PFC lesions throughout behavioural compensation.

3.3. Fractional anisotropy of the thalamocortical white matter tracts

Since FA decreased in the major frontoparietal cortical tracts in the large lesion monkeys at the time of behavioural recovery, we wanted to test whether thalamocortical pathways were instead involved in mediating the improved behaviour and increased frontoparietal resting-state functional connectivity (see Adam et al., 2020) following larger PFC lesions. Thalamocortical fiber tracts were reconstructed using probabilistic tractography and used to extract tract-specific FA values. Average values were calculated across the voxels of each tract and statistically compared between pre-lesion and post-lesion and between early and late post-lesion.

One-way ANOVAs revealed that FA significantly increased in at least one of four thalamocortical fiber tracts in both large lesion monkeys. In Monkey B, FA increased in the contralesional pathway between the mediodorsal thalamus and the PFC and decreased in both pathways between the lateral pulvinar and PPC (Fig. 8A,B). In Monkey F, we found increased FA in both ipsilesional pathways between the mediodorsal thalamus and the PFC and between the lateral pulvinar and PPC (Fig. 8A,B). Thalamocortical tract FA also increased in both small lesion monkeys from early to late post-lesion. In sum, although monkeys with larger PFC lesions had decreased FA in the cortical frontoparietal tracts throughout behavioural recovery, they showed increased FA in thalamocortical fiber tracts which may be providing a compensatory response to return behavioural performance to baseline.

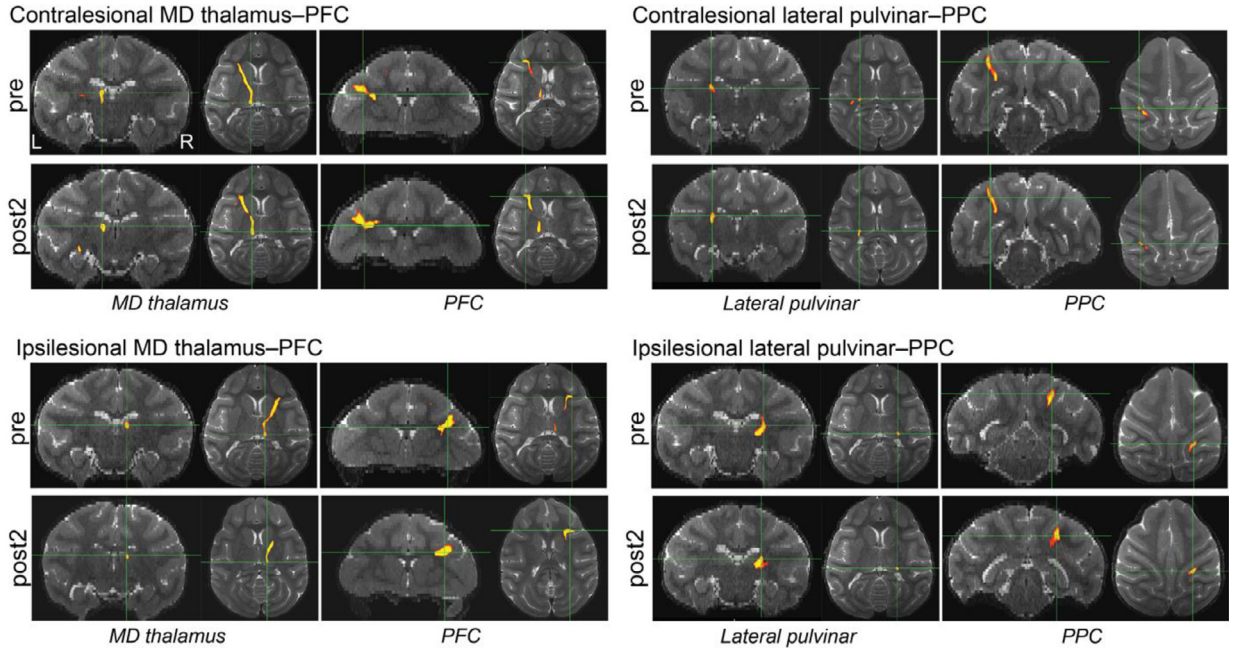

Fig. 6. Representative thalamocortical white matter tracts reconstructed with probabilistic tractography. Thalamocortical tracts are shown in yellow and red and are overlaid onto coronal and axial T2 slices. First column: contralesional and ipsilesional seeds in the mediodorsal thalamus and FEF revealed streamlines connecting the thalamus and PFC that traveled within hemisphere. Second column: contralesional and ipsilesional seeds in the lateral pulvinar and LIP revealed streamlines connecting the thalamus and PPC that traveled within hemisphere. Abbreviations: pre = pre-lesion, post2 = late post-lesion, L = left, R = right, PFC = prefrontal cortex, PPC = posterior parietal cortex, MD = mediodorsal.

4. Discussion

In this longitudinal DWI study, we used probabilistic tractography to investigate tract-specific microstructural changes within a distributed frontoparietal cortical and thalamocortical network after unilateral PFC lesions. We found that tract-specific FA in remote cortical fiber tracts (i.e., contralesional SLF and transcallosal PPC) increased after small lesions (in Monkeys L and S) and decreased after larger lesions (in Monkeys B and F) throughout recovery of contralesional saccade target selection. We also found both increased and decreased FA between thalamic nuclei and frontoparietal cortical areas in both small and large lesion monkeys throughout behavioural recovery. Our findings suggest that cortical and thalamocortical fiber tracts connecting remote areas of the frontoparietal network (i.e., distant to the lesion) may contribute an important compensatory response to support recovery of function after small lesions. In monkeys with larger lesions, decreased FA in cortical tracts and increased FA in thalamocortical tracts suggests that larger PFC lesions may involve recruitment of alternate pathways beyond cortical tracts to support behavioural recovery.

4.1. Microstructural changes in lesion-affected cortical fiber tracts throughout behavioural recovery

First, we discuss white matter degeneration in lesion-affected fiber tracts, including ipsilesional SLF and transcallosal PFC tracts. In the lesion-affected tracts of the two large lesion monkeys, Monkeys B and F, we found *decreased* FA and *increased* mean diffusivity, a pattern of changes also reported in stroke patients (Schaechter et al., 2009; Dacosta-Aguayo et al., 2014; Umarova et al., 2017), and thought to reflect myelin breakdown in axons directly connected to the lesion (Werring et al., 2000; Pierpaoli et al., 2001; Beaulieu, 2002). In contrast, the two small lesions monkeys, Monkeys L and S, showed *increased* FA in these fiber tracts, although these tracts in Monkey S additionally showed *increased* mean diffusivity which is in line with white matter degeneration. Since Monkey L sustained the smallest lesion, spared fibers from the lesioned PFC traveling via ipsilesional SLF or transcallosal fibers may have allowed for optimal neural compensation due to local plasticity (Murphy and Corbett, 2009). While increased FA in ipsilesional SLF and transcallosal PFC tracts in Monkey L may reflect adaptive plasticity supporting behavioural recovery, these findings should be interpreted with caution since DWI changes in lesion-affected tracts may be confounded by lesion pathology (Pierpaoli et al., 2001).

4.2. Transneuronal microstructural changes in remote cortical fiber tracts throughout recovery

Over several days to weeks following the initial degeneration of lesion-affected tracts, remote fibers indirectly connected to the lesion across multiple synapses may undergo transneuronal degeneration (Zhang et al., 2012; Baron et al., 2014; Fornito et al., 2015), the extent of which likely depends on lesion size and location (Wasserman and Schlichter, 2008; Thiel et al., 2010). Transneuronal degeneration may appear on DWI as decreased FA and/or increased mean diffusivity in remote fiber tracts (Beaulieu, 2002), which may reflect decreased fiber density, demyelination, and/or axonal loss (Sotak, 2002).

We found evidence of transneuronal degeneration in the remote fiber tracts examined in this study, contralesional SLF and transcallosal PPC, following large PFC lesions (Monkeys B and F), but not after smaller lesions (Monkeys L and S). Specifically, Monkeys B and F showed decreased FA and increased mean diffusivity in contralesional SLF and transcallosal PPC tracts, evidence of transneuronal degeneration. Several lines of evidence support our finding of decreased FA in remote tracts only after larger lesions with more severe and lasting deficits. DWI studies have reported that, compared to patients with mild or recovered neglect, patients with severe and persistent deficits showed decreased FA in the posterior corpus callosum (isthmus/splenium), which provides communication between bilateral parietal areas (Bozzali et al., 2012; Lunven et al., 2015), or decreased FA between contralesional frontoparietal areas (Umarova et al., 2014). Similarly, in a longitudinal study of neglect, Umarova et al. (2017) reported that the degree

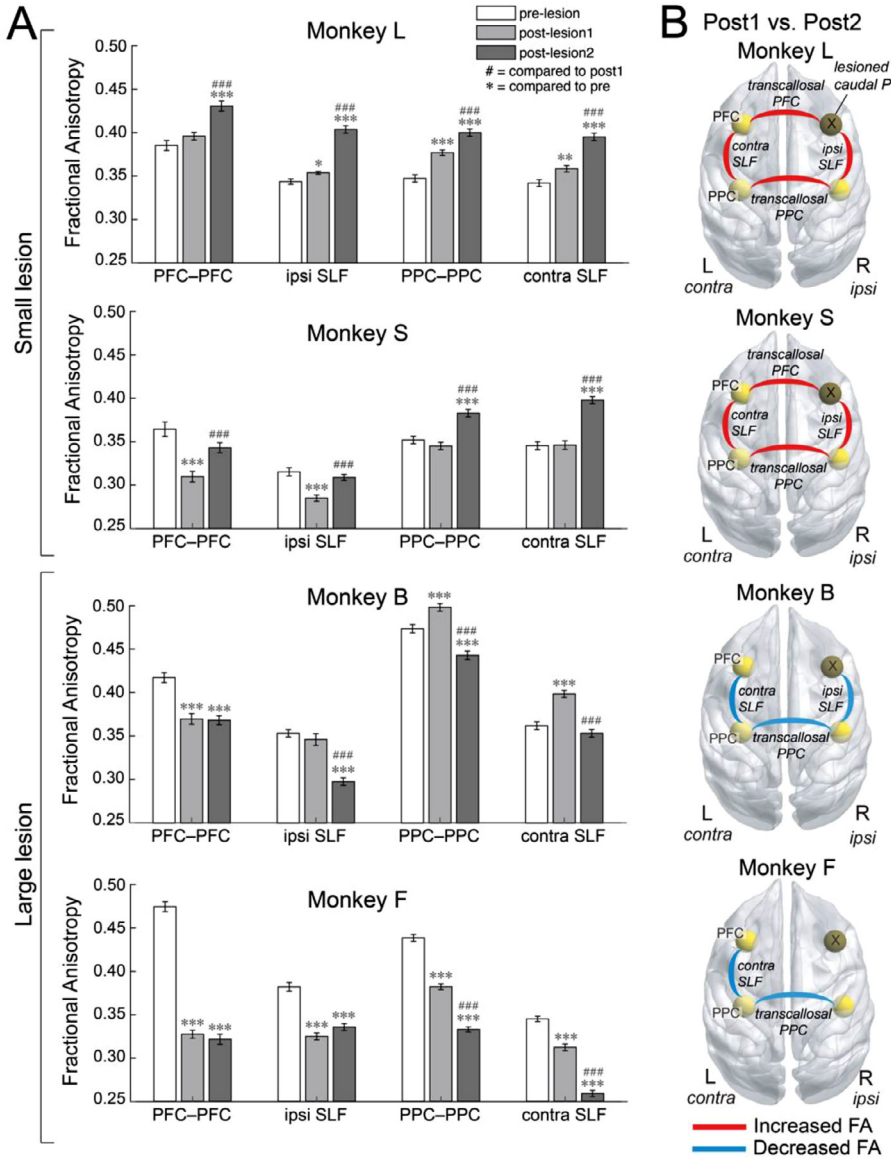

Fig. 7. Changes in fractional anisotropy of cortical fiber tracts over time. (A) White matter tracts of interest were reconstructed with probabilistic tractography and then used to extract tract-specific measures of fractional anisotropy. Statistical comparisons between pre-lesion and post-lesion time points were made using one-way ANOVAs with post-hoc Tukey's tests (* = p<0.05, ** = p<0.01, *** = p<0.001). Statistical comparisons between post-lesion1 and post-lesion2 were made using one-way ANOVAs with post-hoc Tukey's tests (# = p<0.05, ## = p<0.01, ### = p<0.001). Error bars represent standard error of the mean across voxels. (B) Schematic summary of the significant FA changes from post-lesion1 to post-lesion2. Red lines indicate significantly increased FA and solid blue lines indicate significantly decreased FA. Abbreviations: post-lesion1 = week 1 post-lesion, post-lesion2 = week 8 or week 16 post-lesion (behavioural compensation time point), PFC–PFC = transcallosal PFC tract, PPC-PPC = transcallosal PPC tract, SLF = superior longitudinal fasciculus, ipsi = ipsilesional, contra = contralesional.

of unrecovered neglect correlated with degeneration in contralesional frontoparietal white matter (Umarova et al., 2017). In a study of chronic stroke patients recovering from motor-related deficits, poorly-recovered patients showed reduced FA in both ipsilesional and contralesional corticospinal tracts, whereas well-recovered patients showed increased FA in those tracts compared to healthy controls (Schaechter et al., 2009). Alternatively, decreased FA in remote tracts after larger lesions may not necessarily underlie severity or persistence of behavioural deficits, but may instead reflect an epiphenomenon of larger lesions (Umarova et al., 2017).

In contrast, the two small lesion monkeys (Monkeys L and S) showed increased FA in remote contralesional SLF and transcallosal PPC tracts, and Monkey L also showed decreased mean diffusivity in contralesional SLF, which may reflect increased myelination over time (Beaulieu, 2002). Previous studies have highlighted an adaptive role for post-lesion changes in distant white matter in stroke patients (Bütefisch et al., 2003; Crofts et al., 2011) and animal models (Stroemer et al., 1995; Napieralski et al., 1996; Carmichael and Chesselet, 2002; Liu et al., 2008). In patients, improved motor function correlated with increased FA in contralesional white matter (Schaechter et al., 2009; Lin et al., 2015; Liu et al., 2015). Thus, our finding of increased FA in remote fibers after smaller lesions may reflect an adaptive and compensatory change in white matter microstructure possibly related to their faster recovery of function (8 weeks) compared to those with larger lesions (16 weeks).

4.3. *Lesion size-dependent microstructural plasticity in white matter fiber tracts*

One possible explanation for the differences between small and large lesions in the FA of remote fibers may come from variability in the extent of disinhibition and excitotoxicity. Lesions typically induce large-scale depolarization of connected areas resulting in disinhibition and hyperexcitability of widespread networks (Buchkremer-Ratzmann and Witte, 1997; Liepert et al., 2000), which may induce adaptive structural plasticity in the case of small lesions (Jones and Schallert, 1992; Carmichael and Chesselet, 2002; Gonzalez and Kolb, 2003; Reitmeir et al., 2011; Lin et al., 2015). However, larger lesions induce more widespread disinhibition which may lead to greater degeneration across indirectly connected areas due to excitotoxicity and excessive metabolic stress from persistent hyperactivation (Ross and Ebner, 1990; Buchkremer-Ratzmann and Witte, 1997; Saxena and Caroni, 2011; de Haan et al., 2012b).

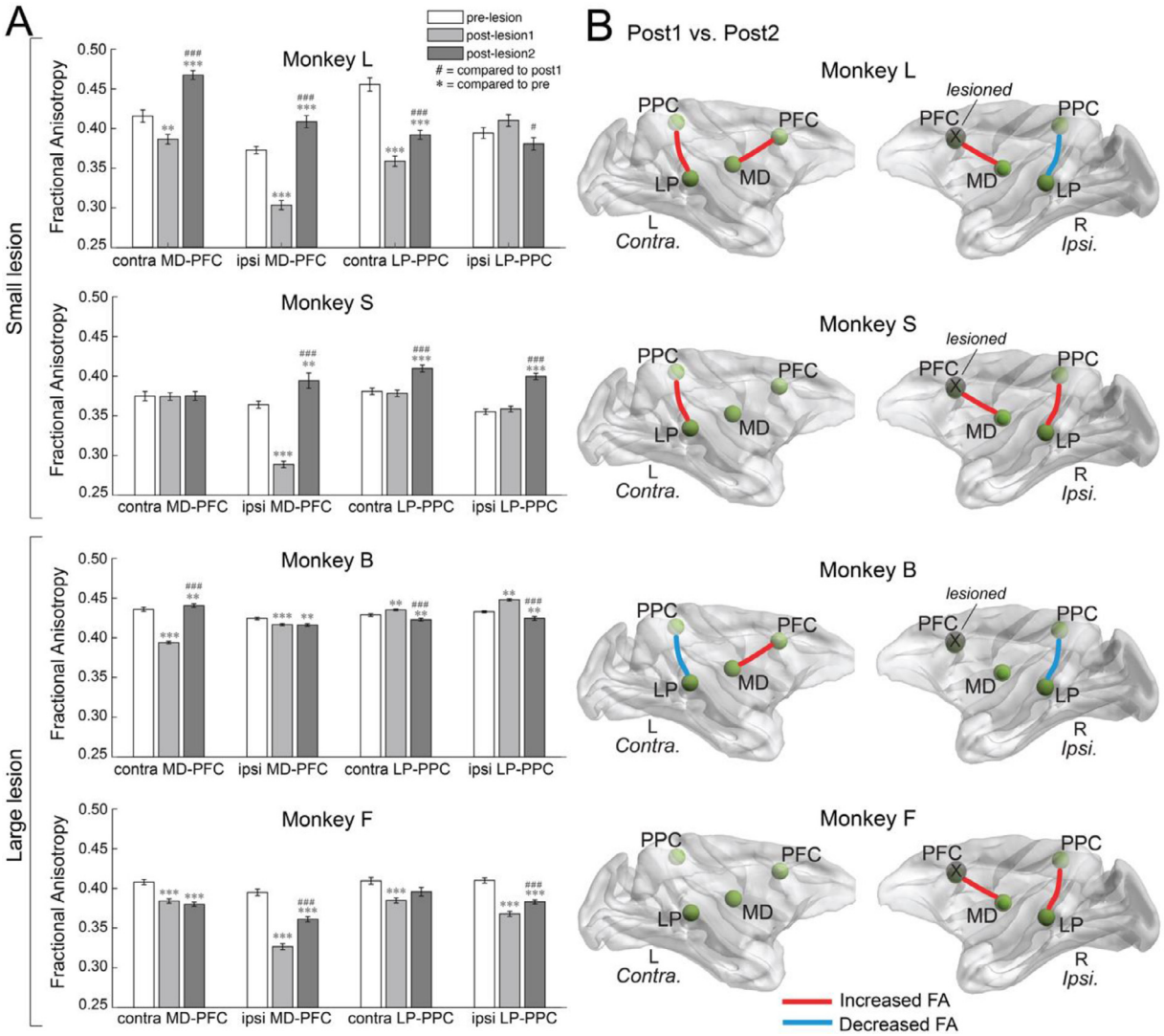

Fig. 8. (A) Changes in the fractional anisotropy of thalamocortical white matter tracts over time. White matter tracts of interest were reconstructed with probabilistic tractography and then used to extract tract-specific measures of fractional anisotropy (FA). (B) Summary schematic showing tracts with significant changes in FA from panel A. Red lines represent tracts with significantly increased FA and blue lines represent tracts with significantly decreased FA at post-lesion compared to pre-lesion. Statistical comparisons between pre-lesion and post-lesion time points were made using one-way ANOVAs with post-hoc Tukey's tests (* = p<0.05, ** = p<0.01, *** = p<0.001). Statistical comparisons between post-lesion1 and post-lesion2 were made using one-way ANOVAs with post-hoc Tukey's tests (# = p<0.05, ## = p<0.01, ### = p<0.001). Error bars represent standard error of the mean across voxels. Abbreviations: post-1 = week 1 post-lesion, post2 = week 8 or week 16 post-lesion (behavioural compensation time point), MD = mediodorsal thalamus, LP = lateral pulvinar, PFC = prefrontal cortex, PPC = posterior parietal cortex, ipsi = ipsilesional, contra = contralesional.

In our companion rsFC paper (Adam et al., 2020), we showed that behavioural performance correlated with increasing rsFC between contralesional PFC and ipsilesional PPC, a functional link that is likely mediated by the contralesional SLF and transcallosal PPC tracts following a unilateral PFC lesion. However, in this study we found that microstructural changes in those white matter tracts differed based on lesion size. Although we found inconsistencies between changes in microstructure and the corresponding rsFC reported in our companion paper (Adam et al., 2020), the magnitude of changes in FA were highly robust. Thus, these discrepancies are unlikely due to methodology, but instead may reflect biological variability in the compensatory response after lesions of different size or that affect different areas. We found that FA increased after small lesions but decreased after larger lesions in the fiber tracts that connect regions with increased rsFC in all four monkeys (i.e., contralesional SLF and transcallosal PPC). We interpret this finding as support for a compensatory role of the contralesional (intact) hemisphere in recovery of function after small lesions. This interpretation is supported by studies showing positive correlations between rsFC and FA in fiber tracts indirectly linking functionally-connected areas (Greicius et al., 2009; Honey et al., 2009; Adachi et al., 2012; Messé et al., 2014; Hori et al., 2020).

However, we did not observe this compensatory increase in FA of remote cortical tracts in large lesion monkeys; we instead found decreased FA in the remote contralesional SLF and transcallosal PPC cortical tracts. One possible explanation comes from accumulating evidence that network reorganization can maintain functional connectivity after loss of major structural pathways. Studies have shown that after major structural disconnection of the corpus callosum, sparing of even a few fibers was sufficient to maintain normal functional connectivity between hemispheres months later (Uddin et al., 2008; Tyszka et al., 2011; O'Reilly et al., 2013; Uddin, 2013). Alternatively, although functional and structural connectivity are often correlated, two regions with

a 'weakened' structural connection (e.g., decreased FA) may show increased rsFC if their structural connectivity with a related third region is strengthened (Koch et al., 2002; Honey et al., 2009). Decreased FA in cortical white matter tracts in Monkeys B and F suggested that behavioural recovery after larger PFC lesions may not be solely mediated by cortical frontoparietal-related tracts. Thus, we examined changes in FA of thalamocortical fiber tracts since thalamic input to the frontoparietal network is one candidate source of compensatory signals relayed from subcortical areas.

4.4. Role of thalamocortical fiber tracts in recovery of function after large PFC lesions

Indeed, we found increased FA in the fiber tract connecting the mediodorsal thalamus with the PFC in the contralesional (intact) hemisphere in Monkey B throughout behavioural recovery. In Monkey F, increased FA was found in the ipsilesional fiber tracts connecting mediodorsal thalamus to the PFC and connecting lateral pulvinar with the PPC. The mediodorsal nucleus of the thalamus and lateral pulvinar have been shown to play a role in visuospatial attention (Petersen et al., 1987; Sommer and Wurtz, 2004), which supports their role in the recovery of saccade target selection. In line with our findings, studies have shown that thalamic input to distinct cortical areas can regulate the neural synchrony and functional connectivity between those cortical regions (Nakajima and Halassa, 2017; Saalmann et al., 2012). Additionally, Zaaimi et al. (2012) showed that subcortical fiber tracts, but not the contralesional corticospinal tract, contributed to the recovery of motor function following extensive unilateral lesions in the macaque corticospinal tract (Zaaimi et al., 2012).

It is worth discussing the finding in Monkey B of increased FA between the mediodorsal thalamus and PFC in the contralesional (intact) hemisphere. Although neurons in the mediodorsal thalamus have been considered to predominantly represent the contralateral visual field, anatomical and electrophysiology studies in macaques provide evidence that mediodorsal thalamus has ipsilateral hemifield representations (Cavanaugh et al., 2020; Watanabe and Funahashi, 2004) and shares connections with contralateral PFC (Dermon and Barbas, 1994; Preuss and Goldman-Rakic, 1987). Watanabe and Funahashi (2004) recorded neural activity in the mediodorsal thalamus of macaques performing an oculomotor delayed response task and found a significant contralateral hemifield bias during cue-period and presaccadic activity. However, about one-third of neurons with cue-period, delay-period, or presaccadic activity preferred the ipsilateral hemifield (Watanabe and Funahashi, 2004). More recently, Cavanaugh et al. (2020) found neurons in the mediodorsal thalamus with presaccadic activity to both contralateral and ipsilateral visual fields. Although there are fewer ipsilaterally-tuned than contralaterally-tuned neurons, post-lesion brain plasticity may serve to stimulate activity in ipsilaterally-tuned neurons as a compensatory mechanism for recovering function. Moreover, anatomical studies in macaques have also shown that the mediodorsal thalamus shares reciprocal connections with bilateral PFC (Dermon and Barbas, 1994; Preuss and Goldman-Rakic, 1987). Altogether, although it may be surprising to see increased FA in the intact hemisphere during recovery of a contralesional deficit (ipsilateral hemifield for the intact hemisphere), this result may be explained by considering the role of the intact hemisphere in ipsilateral (contralesional) saccade target selection.

Future studies may consider directly testing the role of thalamocortical connections in the recovery of function after large PFC lesions using neuroimaging techniques or inactivation methods. Lastly, since DWI is limited in its ability to detect true white matter fiber structure, future research may opt to use a contrast agent (e.g., manganese) during MR imaging for a better approximation of the structural connectivity *in vivo* (Schaeffer et al., 2018).

Data and code availability statement

The data and code that support the findings of this study are available from the Authors upon reasonable request.

Author contributions

Ramina Adam: Conceptualization, Methodology, Software, Formal analysis, Investigation, Data curation, Writing – Original Draft, Writing – Review & Editing, Visualization, Project administration; ***David J. Schaeffer***: Conceptualization, Methodology, Writing – Review & Editing; ***Kevin Johnston***: Methodology, Software, Writing – Review & Editing; ***Ravi S. Menon***: Conceptualization, Methodology, Writing – Review & Editing, Funding acquisition; ***Stefan Everling***: Conceptualization, Methodology, Resources, Writing – Review & Editing, Supervision, Funding acquisition

Funding

This research was supported by the Canadian Institutes of Health Research grant FRN148365 to S.E., the Canada First Research Excellence Fund to BrainsCAN, and Brain Canada to R.S.M. R.A. was supported by the Ontario Graduate Scholarship and the Canada Graduate Scholarship-Master's (CGS-M).

Declarations of Competing Interest

The authors declare no competing financial or non-financial interests.

Acknowledgments

We thank Joseph Gati and Trevor Szekeres for technical support and assistance with MRI acquisition; Nicole Hague and Ashley Kirley for animal care and preparation; and Kyle Gilbert for designing the macaque RF coil.

Supplementary materials

Supplementary material associated with this article can be found, in the online version, at doi:10.1016/j.neuroimage.2021.117919.

References

Adachi, Y, Osada, T, Sporns, O, Watanabe, T, Matsui, T, Miyamoto, K, Miyashita, Y, 2012. Functional connectivity between anatomically unconnected areas is shaped by collective network-level effects in the macaque cortex. Cereb. Cortex 22, 1586–1592.

Adam, R, Johnston, K, Everling, S, 2019. Recovery of contralesional saccade choice and reaction time deficits after a unilateral endothelin-1-induced lesion in the macaque caudal prefrontal cortex. J. Neurophysiol. 122, 672–690.

Adam, R, Johnston, K, Menon, RS, Everling, S, 2020. Functional reorganization during the recovery of contralesional target selection deficits after prefrontal cortex lesions in macaque monkeys. Neuroimage 207, 116339.

Alexander, A, Lee, J, Lazar, M, Field, A, 2007. Diffusion tensor imaging of the brain. Neurother 4, 316–329.

Andersson, JLR, Sotiropoulos, SN, 2016. An integrated approach to correction for off-resonance effects and subject movement in diffusion MR imaging. Neuroimage 125, 1063–1078.

Asanuma, C., Andersen, R.A., Cowan, W.M., 1985. The thalamic relations of the caudal inferior parietal lobule and the lateral prefrontal cortex in monkeys: divergent cortical projections from cell clusters in the medial pulvinar nucleus. J. Comp. Neurol. 241, 357–381.

Baizer, J.S., Robert, D., Ungerleider, L.G., 1993. Comparison of subcortical connections of inferior temporal and posterior parietal cortex in monkeys. Vis. Neurosci..

Baldassarre, A, Ramsey, LE, Hacker, CL, Callejas, A, Astafiev, S.V., Metcalf, N.V., Zinn, K, Rengachary, J, Snyder, AZ, Carter, AR, Shulman, GL, Corbetta, M, Zinn, K, Siegel, JS, Metcalf, N.V., M., S, Snyder, AZ, Corbetta, M, 2014. Large-scale changes in network interactions as a physiological signature of spatial neglect. Brain 137, 3267–3283.

Barbas, H., Mesulam, M.-M, 1981. Organization of afferent input to subdivisions of area 8 in the rhesus monkey. J. Comp. Neurol. 200, 407–431.

Barbas, H, Pandya, D, 1984. Topography of commissural fibers of the prefrontal cortex in the rhesus monkey. Exp. Brain Res. 55, 187–191.

Baron, JC, Yamauchi, H, Fujioka, M, Endres, M, 2014. Selective neuronal loss in ischemic stroke and cerebrovascular disease. J. Cereb. Blood Flow Metab. 34, 2–18.
Bartolomeo, P, 2007. Visual neglect. Curr. Opin. Neurol. 20, 381–386.
Bartolomeo, P, Thiebaut de Schotten, M, Chica, AB, 2012. Brain networks of visuospatial attention and their disruption in visual neglect. Front. Hum. Neurosci. 6, 1–10.
Basser, P, Mattiello, J, LeBihan, D, 1994. MR diffusion tensor spectroscopy and imaging. Biophys. J. 66, 259–267.
Basser, P, Pierpaoli, C, 1996. Microstructural and physiological features of tissues elucidated by quantitative-diffusion-tensor MRI. J. Magn. Reson. 111, 209–219.
Beaulieu, C, 2002. The basis of anisotropic water diffusion in the nervous system - A technical review. NMR Biomed. 15, 435–455.
Behrens, TEJ, Berg, HJ, Jbabdi, S, Rushworth, MFS, Woolrich, MW, 2007. Probabilistic diffusion tractography with multiple fibre orientations: What can we gain? Neuroimage 34, 144–155.
Behrens, TEJ, Johansen-Berg, H, Woolrich, MW, Smith, SM, Wheeler-Kingshott, CAM, Boulby, PA, Barker, GJ, Sillery, EL, Sheehan, K, Ciccarelli, O, Thompson, AJ, Brady, JM, Matthews, PM, 2003a. Non-invasive mapping of connections between human thalamus and cortex using diffusion imaging. Nat. Neurosci. 6, 750–757.
Behrens, TEJ, Woolrich, MW, Jenkinson, M, Johansen-Berg, H, Nunes, RG, Clare, S, Matthews, PM, Brady, JM, Smith, SM, 2003b. Characterization and propagation of uncertainty in diffusion-weighted MR imaging. Magn. Reson. Med. 50, 1077–1088.
Bennett, IJ, Madden, DJ, Vaidya, CJ, Howard, JH, Howard, D.V., 2011. White matter integrity correlates of implicit sequence learning in healthy aging. Neurobiol. Aging 32, 2317 e1-2317.e12.
Bozzali, M, Mastropasqua, C, Cercignani, M, Giulietti, G, Bonnì, S, Caltagirone, C, Koch, G, 2012. Microstructural damage of the posterior corpus callosum contributes to the clinical severity of neglect. PLoS One 7, 3–8.
Buchkremer-Ratzmann, I, Witte, OW, 1997. Extended brain disinhibition following small photothrombotic lesions in rat frontal cortex. Neuroreport 8, 519–522.
Bütefisch, CM, Netz, J, Weßling, M, Seitz, RJ, Hömberg, V, 2003. Remote changes in cortical excitability after stroke. Brain 126, 470–481.
Carmichael, ST, Chesselet, MF, 2002. Synchronous neuronal activity is a signal for axonal sprouting after cortical lesions in the adult. J. Neurosci. 22, 6062–6070.
Cavanaugh, J, McAlonan, K, Wurtz, RH, 2020. Organization of corollary discharge neurons in monkey medial dorsal thalamus. J. Neurosci. 40, 6367–6378.
Celik, A, 2016. Effect of imaging parameters on the accuracy of apparent diffusion coefficient and optimization strategies. Diagnostic Interv. Radiol. 22, 101–107.
Corbetta, M, Shulman, GL, 2011. Spatial neglect and attention networks. Annu. Rev. Neurosci. 34, 569–599.
Crofts, JJ, Higham, DJ, Bosnell, R, Jbabdi, S, Matthews, PM, Behrens, TEJ, Johansen-Berg, H, 2011. Network analysis detects changes in the contralesional hemisphere following stroke. Neuroimage 54, 161–169.
Cunningham, SI, Tomasi, D, Volkow, ND, 2017. Structural and functional connectivity of the precuneus and thalamus to the default mode network. Hum. Brain Mapp. 38, 938–956.
Dacosta-Aguayo, R, Graña, M, Fernández-Andújar, M, López-Cancio, E, Cáceres, C, Bargalló, N, Barrios, M, Clemente, I, Monserrat, PT, Sas, MA, Dávalos, A, Auer, T, Mataró, M, 2014. Structural integrity of the contralesional hemisphere predicts cognitive impairment in ischemic stroke at three months. PLoS One 9, 1–11.
Dai, P, Huang, H, Zhang, L, He, J, Zhao, X, Yang, F, Zhao, N, Yang, J, Ge, L, Lin, Y, Yu, H, Wang, J, 2017. A pilot study on transient ischemic stroke induced with endothelin-1 in the rhesus monkeys. Sci. Rep. 7, 45097.
Damoiseaux, JS, Greicius, MD, 2009. Greater than the sum of its parts: a review of studies combining structural connectivity and resting-state functional connectivity. Brain Struct. Funct. 213, 525–533.
de Haan, B, Karnath, HO, Driver, J, 2012a. Mechanisms and anatomy of unilateral extinction after brain injury. Neuropsychologia 50, 1045–1053.
de Haan, W, Mott, K, van Straaten, ECW, Scheltens, P, Stam, CJ, 2012b. Activity dependent degeneration explains hub vulnerability in alzheimer's disease. PLoS Comput. Biol. 8.
Dermon, CR, Barbas, H, 1994. Contralateral thalamic projections predominantly reach transitional cortices in the rhesus monkey. J. Comp. Neurol. 344, 508–531.
Deuel, R, Collins, R, 1983. Recovery from unilateral neglect. Exp. Neurol. 81, 733–748.
Di Pellegrino, G, Basso, G, Frassinetti, F, 1997. Spatial extinction on double asynchronous stimulation. Neuropsychologia 35, 1215–1223.
Dijkhuizen, RM, van der Marel, K, Otte, WM, Hoff, EI, van der Zijden, JP, van der Toorn, A, van Meer, MPA, 2012. Functional MRI and diffusion tensor imaging of brain reorganization after experimental stroke. Transl. Stroke Res. 3, 36–43.
Fornito, A, Zalesky, A, Breakspear, M, 2015. The connectomics of brain disorders. Nat. Rev. Neurosci. 16, 159–172.
Galantucci, S, Tartaglia, MC, Wilson, SM, Henry, ML, Filippi, M, Agosta, F, Dronkers, NF, Henry, RG, Ogar, JM, Miller, BL, Gorno-Tempini, ML, 2011. White matter damage in primary progressive aphasias: a diffusion tensor tractography study. Brain 134, 3011–3029.
Ge, H, Yin, X, Xu, J, Tang, Y, Han, Y, Xu, W, Pang, Z, Meng, H, Liu, S, 2013. Fiber pathways of attention subnetworks revealed with tract-based spatial statistics (TBSS) and probabilistic tractography. PLoS One 8, 1–7.
Gilbert, KM, Gati, JS, Barker, K, Everling, S, Menon, RS, 2016. Optimized parallel transmit and receive radiofrequency coil for ultrahigh-field MRI of monkeys. Neuroimage 125, 153–161.
Goldman-Rakic, P.S., Porrino, L.J., 1985. The primate mediodorsal (MD) nucleus and its projection to the frontal lobe. J. Comp. Neurol. 242, 535–560.
Gonzalez, CLR, Kolb, B, 2003. A comparison of different models of stroke on behaviour and brain morphology. Eur. J. Neurosci. 18, 1950–1962.
Gray, DT, Umapathy, L, Burke, SN, Trouard, TP, Barnes, CA, 2018. Tract-specific white matter correlates of age-related reward devaluation deficits in macaque monkeys. J. Neuroimaging Psychiatry Neurol. 03, 13–26.
Greicius, MD, Supekar, K, Menon, V, Dougherty, RF, 2009. Resting-state functional connectivity reflects structural connectivity in the default mode network. Cereb. Cortex 19, 72–78.
Hagmann, P, Cammoun, L, Gigandet, X, Meuli, R, Honey, CJ, Van Wedeen, J, Sporns, O, 2008. Mapping the structural core of human cerebral cortex. PLoS Biol. 6, 1479–1493.
He, BJ, Snyder, AZ, Vincent, JL, Epstein, A, Shulman, GL, Corbetta, M, 2007. Breakdown of functional connectivity in frontoparietal networks underlies behavioral deficits in spatial neglect. Neuron 53, 905–918.
Herbert, WJ, Powell, K, Buford, JA, 2015. Evidence for a role of the reticulospinal system in recovery of skilled reaching after cortical stroke: initial results from a model of ischemic cortical injury. Exp. Brain Res. 233, 3231–3251.
Hofer, S, Frahm, J, 2008. In vivo mapping of fiber pathways in the rhesus monkey brain. Open Med. Imaging J. 2, 32–41.
Hofer, S, Merboldt, KD, Tammer, R, Frahm, J, 2008. Rhesus monkey and human share a similar topography of the corpus callosum as revealed by diffusion tensor mri in vivo. Cereb. Cortex 18, 1079–1084.
Honey, CJ, Sporns, O, Cammoun, L, Gigandet, X, Thiran, JP, Meuli, R, Hagmann, P, 2009. Predicting human resting-state functional connectivity from structural connectivity. Proc. Natl. Acad. Sci. U. S. A. 106, 2035–2040.
Hori, Y, Schaeffer, DJ, Gilbert, KM, Hayrynen, LK, Cléry, JC, Gati, JS, Menon, RS, Everling, S, 2020. Comparison of resting-state functional connectivity in marmosets with tracer-based cellular connectivity. Neuroimage 204.
Jenkinson, M, Bannister, P, Brady, M, Smith, S, 2002. Improved optimization for the robust and accurate linear registration and motion correction of brain images. Neuroimage 17, 825–841.
Johnston, K, Lomber, SG, Everling, S, 2016. Unilateral deactivation of macaque dorsolateral prefrontal cortex induces biases in stimulus selection. J. Neurophysiol. 115, 1468–1476.
Jones, TA, Schallert, T, 1992. Overgrowth and pruning of dendrites in adult rats recovering from neocortical damage. Brain Res. 581, 156–160.
Kievit, J., Kuypers, H.G.J.M., 1977. Organization of the thalamo-cortical connexions to the frontal lobe in the rhesus monkey. Exp. Brain Res. 29, 299–322.
Koch, MA, Norris, DG, Hund-Georgiadis, M, 2002. An investigation of functional and anatomical connectivity using magnetic resonance imaging. Neuroimage 16, 241–250.
Latto, R, Cowey, A, 1971. Visual field defects after frontal eye field lesions in monkeys. Brain Res. 30, 1–24.
Latzman, RD, Taglialatela, JP, Hopkins, WD, 2015. Delay of gratification is associated with white matter connectivity in the dorsal prefrontal cortex: a diffusion tensor imaging study in chimpanzees (Pan troglodytes). Proc. R Soc. B Biol. Sci. 282.
Lewis, JW, Van Essen, DC, 2000. Corticocortical connections of visual, sensorimotor, and multimodal processing areas in the parietal lobe of the macaque monkey. J. Comp. Neurol. 428, 112–137.
Li, K, Malhotra, PA, 2015. Spatial neglect. Pract. Neurol. 15, 333–339.
Liepert, J, Storch, P, Fritsch, A, Weiller, C, 2000. Motor cortex disinhibition in acute stroke. Clin. Neurophysiol. 111, 671–676.
Lin, YC, Daducci, A, Meskaldji, DE, Thiran, JP, Michel, P, Meuli, R, Krueger, G, Menegaz, G, Granziera, C, 2015. Quantitative analysis of myelin and axonal remodeling in the uninjured motor network after stroke. Brain Connect. 5, 401–412.
Lindenberg, R, Zhu, LL, Rüber, T, Schlaug, G, 2012. Predicting functional motor potential in chronic stroke patients using diffusion tensor imaging. Hum. Brain Mapp. 33, 1040–1051.
Liu, G, Dang, C, Chen, X, Xing, S, Dani, K, Xie, C, Peng, K, Zhang, J, Li, J, Zhang, J, Chen, L, Pei, Z, Zeng, J, 2015. Structural remodeling of white matter in the contralesional hemisphere is correlated with early motor recovery in patients with subcortical infarction. Restor. Neurol. Neurosci. 33, 309–319.
Liu, Z, Li, Y, Zhang, X, Savant-Bhonsale, S, Chopp, M, 2008. Contralesional axonal remodeling of the corticospinal system in adult rats after stroke and bone marrow stromal cell treatment. Stroke 39, 2571–2577.
Lunven, M, De Schotten, MT, Bourlon, C, Duret, C, Migliaccio, R, Rode, G, Bartolomeo, P, 2015. White matter lesional predictors of chronic visual neglect: a longitudinal study. Brain 138, 746–760.
Lynch, JC, Mclaren, JAYW, 1989. Deficits of visual attention and saccadic eye movements after lesions of parietooccipital cortex in monkeys. J. Neurophysiol. 6, 74–90.
Messé, A, Rudrauf, D, Benali, H, Marrelec, G, 2014. Relating structure and function in the human brain: relative contributions of anatomy, stationary dynamics, and non-stationarities. PLoS Comput. Biol. 10.
Mesulam, M-M, 1999. Spatial attention and neglect: parietal, frontal and cingulate contributions to the mental representation and attentional targeting of salient extrapersonal events. Philos. Trans. R. Soc. Lond. B Biol. Sci. 354, 1325–1346.
Murata, Y, Higo, N, 2016. Development and characterization of a macaque model of focal internal capsular infarcts. PLoS One 11, e0154752.
Murphy, TH, Corbett, D, 2009. Plasticity during stroke recovery: from synapse to behaviour. Nat. Rev. Neurosci. 10, 861–872.
Nakajima, M, Halassa, MM, 2017. Thalamic control of functional cortical connectivityt. Curr. Opin. Neurobiol. 44, 127–131.
Napieralski, JA, Butler, AK, Chesselet, MF, 1996. Anatomical and functional evidence for lesion-specific sprouting of corticostriatal input in the adult rat. J. Comp. Neurol. 373, 484–497.
O'Reilly, JX, Croxson, PL, Jbabdi, S, Sallet, J, Noonan, MP, Mars, RB, Browning, PGF, Wilson, CRE, Mitchell, AS, Miller, KL, Rushworth, MFS, Baxter, MG, 2013. Causal effect of disconnection lesions on interhemispheric functional connectivity in rhesus monkeys. Proc. Natl. Acad. Sci. U. S. A. 110, 13982–13987.
Paxinos, G, Huang, X, Toga, A, 2000. The Rhesus Monkey Brain in Stereotaxic Coordinates. Academic Press.

Petersen, S.E., Robinson, D.L., Morris, J.D., 1987. Contributions of the pulvinar to visual spatial attention. Neuropsychologia 25, 97–105.
Petrides, M, Pandya, DN, 1984. Projections to the frontal cortex from the posterior parietal region in the rhesus monkey. J. Comp. Neurol. 116, 105–116.
Pierpaoli, C, Barnett, A, Pajevic, S, Chen, R, Penix, LR, Virta, A, Basser, P, 2001. Water diffusion changes in wallerian degeneration and their dependence on white matter architecture. Neuroimage 13, 1174–1185.
Preuss, TM, Goldman-Rakic, PS, 1987. Crossed corticothalamic and thalamocortical connections of macaque prefrontal cortex. J. Comp. Neurol. 257 269–28.
Provenzale, JM, Taylor, BA, Wilde, EA, Boss, M, Schneider, W, 2018. Analysis of variability of fractional anisotropy values at 3T using a novel diffusion tensor imaging phantom. Neuroradiol. J. 31, 581–586.
Ramsey, LE, Siegel, JS, Baldassarre, A, Metcalf, N.V., Zinn, K, Shulman, GL, Corbetta, M, 2016. Normalization of network connectivity in hemispatial neglect recovery. Ann. Neurol. 80, 127–141.
Reitmeir, R, Kilic, E, Kilic, Ü, Bacigaluppi, M, Elali, A, Salani, G, Pluchino, S, Gassmann, M, Hermann, DM, 2011. Post-acute delivery of erythropoietin induces stroke recovery by promoting perilesional tissue remodelling and contralesional pyramidal tract plasticity. Brain 134, 84–99.
Ross, DT, Ebner, FF, 1990. Thalamic retrograde degeneration following cortical injury: An excitotoxic process? Neuroscience 35, 525–550.
Saalmann, YB, Pinsk, MA, Wang, L, Li, X, Kastner, S, 2012. The pulvinar regulates information transmission between cortical areas based on attention demands. Science 337, 753–756.
Saleem, KS, Logothetis, NK, 2006. A Combined MRI and Histology Atlas of the Rhesus Monkey Brain in Stereotaxic Coordinates.
Sani, I, McPherson, BC, Stemmann, H, Pestilli, F, Freiwald, WA, 2019. Functionally defined white matter of the macaque monkey brain reveals a dorso-ventral attention network. Elife 8, 1–21.
Saxena, S, Caroni, P, 2011. Selective neuronal vulnerability in neurodegenerative diseases: from stressor thresholds to degeneration. Neuron 71, 35–48.
Schaechter, JD, Fricker, ZP, Perdue, KL, Helmer, KG, Vangel, MG, Greve, DN, Makris, N, 2009. Microstructural status of ipsilesional and contralesional corticospinal tract correlates with motor skill in chronic stroke patients. Hum. Brain Mapp. 30, 3461–3474.
Schaeffer, DJ, Adam, R, Gilbert, KM, Gati, JS, Li, AX, Menon, RS, Everling, S, 2017. Diffusion weighted tractography in the common marmoset monkey at 9.4 T. J. Neurophysiol. 118, 1344–1354.
Schaeffer, DJ, Johnston, KD, Gilbert, KM, Gati, JS, Menon, RS, Everling, S, 2018. In vivo manganese tract tracing of frontal eye fields in rhesus macaques with ultra-high field MRI: comparison with DWI tractography. Neuroimage 181, 211–218.
Schiller, PH, Chou, I, 1998. The effects of frontal eye field and dorsomedial frontal cortex lesions on visually guided eye movements. Nat. Neurosci. 1, 248–253.
Schmahmann, JD, Pandya, DN, Wang, R, Dai, G, D'Arceuil, HE, De Crespigny, AJ, Wedeen, VJ, 2007. Association fibre pathways of the brain: Parallel observations from diffusion spectrum imaging and autoradiography. Brain 130, 630–653.
Selemon, L.D., Goldman-Rakic, P.S., 1988. Common cortical and subcortical targets of the dorsolateral prefrontal and posterior parietal cortices in the rhesus monkey: evidence for a distributed neural network subserving spatially guided behavior. J. Neurosci. 8, 4049–4068.
Shen, K, Hutchison, RM, Bezgin, G, Everling, S, McIntosh, AR, 2015. Network structure shapes spontaneous functional connectivity dynamics. J. Neurosci. 35, 5579–5588.
Sommer, M.A., Wurtz, R.H., 2004. What the brain stem tells the frontal cortex. I. Oculomotor signals sent from superior colliculus to frontal eye field via mediodorsal thalamus. J. Neurophysiol. 91, 1381–1402.
Sotak, CH, 2002. The role of diffusion tensor imaging in the evaluation of ischemic brain - A review. NMR Biomed. 15, 561–569.
Stroemer, RP, Kent, TA, Hulsebosch, CE, 1995. Neocortical neural sprouting, synaptogenesis, and behavioral recovery after neocortical infarction in rats. Stroke 26, 2135–2144.
Tehovnik, EJ, Sommer, M a., Chou, IH, Slocum, WM, Schiller, PH, 2000. Eye fields in the frontal lobes of primates. Brain Res. Rev. 32, 413–448.
Teo, L, Bourne, J, 2014. A Reproducible and Translatable Model of Focal Ischemia in the Visual Cortex of Infant and Adult Marmoset Monkeys. Brain Pathol. 24, 459–474.
Thiebaut de Schotten, M, Dell'Acqua, F, Valabregue, R, Catani, M, 2012. Monkey to human comparative anatomy of the frontal lobe association tracts. Cortex 48, 82–96.
Thiel, A, Radlinska, BA, Paquette, C, Sidel, M, Soucy, JP, Schirrmacher, R, Minuk, J, 2010. The temporal dynamics of poststroke neuroinflammation: A longitudinal diffusion tensor imaging-guided PET study with 11C-PK11195 in acute subcortical stroke. J. Nucl. Med. 51, 1404–1412.
Tobias, TJ, 1975. Afferents to prefrontal cortex from the thalamic mediodorsal nucleus in the rhesus monkey. Brain Res. 83, 191–212.
Tyszka, MJ, Kennedy, DP, Adolphs, R, Paul, LK, 2011. Intact bilateral resting-state networks in the absence of the corpus callosum. J. Neurosci. 31, 15154–15162.
Uddin, LQ, 2013. Complex relationships between structural and functional brain connectivity. Trends Cogn. Sci. 17, 600–602.
Uddin, LQ, Mooshagian, E, Zaidel, E, Scheres, A, Margulies, DS, Kelly, AMC, Shehzad, Z, Adelstein, JS, Castellanos, FX, Biswal, BB, Milham, MP, 2008. Residual functional connectivity in the split-brain revealed with resting-state functional MRI. Neuroreport 19, 703–709.
Umarova, RM, Beume, L, Reisert, M, Kaller, CP, Klöppel, S, Mader, I, Glauche, V, Kiselev, VG, Catani, M, Weiller, C, 2017. Distinct white matter alterations following severe stroke. Neurology 88, 1546–1555.
Umarova, RM, Nitschke, K, Kaller, CP, Klöppel, S, Beume, L, Mader, I, Martin, M, Hennig, J, Weiller, C, 2016. Predictors and signatures of recovery from neglect in acute stroke. Ann. Neurol. 79, 673–686.
Umarova, RM, Reisert, M, Beier, TU, Kiselev, VG, Klöppel, S, Kaller, CP, Glauche, V, Mader, I, Beume, L, Hennig, J, Weiller, C, 2014. Attention-network specific alterations of structural connectivity in the undamaged white matter in acute neglect. Hum. Brain Mapp. 35, 4678–4692.
Umarova, RM, Saur, D, Kaller, CP, Vry, MS, Glauche, V, Mader, I, Hennig, JJ, Weiller, C, 2011. Acute visual neglect and extinction: distinct functional state of the visuospatial attention system. Brain 134, 3310–3325.
Wardak, C, Ibos, G, Duhamel, J-RR, Olivier, E, 2006. Contribution of the monkey frontal eye field to covert visual attention. J. Neurosci. 26, 4228–4235.
Wardak, C, Olivier, E, Duhamel, J-R, 2002. Saccadic target selection deficits after lateral intraparietal area inactivation in monkeys. J. Neurosci. 22, 9877–9884.
Wardak, C, Olivier, E, Duhamel, JR, 2004. A Deficit in covert attention after parietal cortex inactivation in the monkey. Neuron 42, 501–508.
Wardak, C, Olivier, E, Duhamel, JR, 2011. The relationship between spatial attention and saccades in the frontoparietal network of the monkey. Eur. J. Neurosci. 33, 1973–1981.
Wasserman, JK, Schlichter, LC, 2008. White matter injury in young and aged rats after intracerebral hemorrhage. Exp. Neurol. 214, 266–275.
Watanabe, Y, Funahashi, S, 2004. Neuronal activity throughout the primate mediodorsal nucleus of the thalamus during oculomotor delayed-responses. I. cue-, delay-, and response-period activity. J. Neurophysiol. 92, 1738–1755.
Werring, DJ, Toosy, AT, Clark, CA, Parker, GJM, Barker, GJ, Miller, DH, Thompson, AJ, 2000. Diffusion tensor imaging can detect and quantify corticospinal tract degeneration after stroke. J. Neurol. Neurosurg. Psychiatry 69, 269–272.
Wilke, M, Kagan, I, Andersen, R, 2012. Functional imaging reveals rapid reorganization of cortical activity after parietal inactivation in monkeys. Proc. Natl Acad. Sci. 109, 8274–8279.
Zaaimi, B, Edgley, SA, Soteropoulos, DS, Baker, SN, 2012. Changes in descending motor pathway connectivity after corticospinal tract lesion in macaque monkey. Brain 135, 2277–2289.
Zakszewski, E, Adluru, N, Tromp, DPM, Kalin, N, Alexander, AL, 2014. A diffusion-tensor-based white matter atlas for rhesus macaques. PLoS One 9 (9), e107398.
Zhang, J, Zhang, Y, Xing, S, Liang, Z, Zeng, J, 2012. Secondary neurodegeneration in remote regions after focal cerebral infarction: a new target for stroke management? Stroke 43, 1700–1705.